Nonlinear spectral phase induced by optical parametric chirped-pulse amplification

Bingjie Zhou,[1] Jingui Ma,[1,*] Jing Wang,[1] Daolong Tang,[1] Guoqiang Xie,[1] Peng Yuan,[1] Heyuan Zhu,[2] and Liejia Qian[1,†]

[1]*Key Laboratory for Laser Plasma (Ministry of Education), School of Physics and Astronomy, Collaborative Innovation Center of IFSA (CICIFSA), Shanghai Jiao Tong University, Shanghai 200240, China*

[2]*Shanghai Engineering Research Center of Ultra-Precision Optical Manufacturing, Department of Optical Science and Engineering, Fudan University, Shanghai 200433, China*

(Received 19 October 2016; published 29 March 2017)

Optical parametric phase (OPP), inherently induced in optical parametric chirped-pulse amplification (OPCPA), will significantly degrade pulse compression in the few-cycle pulse regime. While OPP is a well-known nonlinear phenomenon, its nonlinearity origin has remained unclear in physics. Here, we present a systematic theoretical investigation on OPP and demonstrate that OPP originates from the cascaded quadratic nonlinearity in a broadband OPCPA with intrinsic phase-mismatch. Because the intrinsic phase-mismatch is frequency dependent, OPP manifests itself as a nonlinear spectral phase. We show that OPP increases with the parametric gain, approaches to half the intrinsic phase-mismatch in the high-gain limit, and thus directly links with the crystal dispersion. We also find that the effect of OPP in the spatial domain is typically negligible, which makes the OPP compensation necessary only in the spectral domain. The results presented in this paper are of importance to guide the design of few-cycle intense OPCPA systems.

DOI: 10.1103/PhysRevA.95.033841

I. INTRODUCTION

The generation of few-cycle optical pulses has enabled rapid progress in ultrafast science and attosecond physics [1–3]. Further attractive developments in these areas would benefit from the availability of intense few-cycle laser sources. Therefore, there is a strong quest for broadband amplification schemes to amplify few-cycle pulses. One promising scheme is optical parametric chirped-pulse amplification (OPCPA) [4,5], which combines the technologies of optical parametric amplification (OPA) and chirped-pulse amplification (CPA). The bandwidth of OPCPA can be typically made as large as 100–200 nm, in the visible and near-infrared region, by using the noncollinear phase-matching (PM) configuration [6–8]. So far, sub-three-cycle OPCPA systems have been widely demonstrated in both near-infrared and mid-infrared wavelength regions [9–11]. To further enhance the amplification bandwidth and efficiency, several variants of OPCPA have been also explored, which include frequency domain OPA [12], adiabatic OPA [13,14], and quasiparametric amplification [15].

In contrast to traditional Ti:sapphire CPA lasers, the amplified signal pulses from OPCPA inherently suffer excess spectral-phase distortions besides the accumulated linear phase from the crystal dispersion. In a broadband OPCPA, only the central frequency of the signal satisfies the perfect PM condition, and other frequency components will inevitably experience a frequency-dependent phase-mismatch (intrinsic phase-mismatch). This intrinsic phase-mismatch adds an excess spectral-phase distortion to the signal in OPCPA [16–20]. Such optical parametric phase (OPP) hampers ideal compression of chirped signal pulses and necessitates additional dispersion control on signal pulses. OPP was first theoretically suggested by Ross *et al.* [16] and later on observed in OPCPA experiments [17–19]. OPP exists only under a nonideal PM condition, varies with the pump intensity, and behaves as a nonlinear spectral phase. Several crucial questions are then raised: (1) what is the source of nonlinearity that governs the OPP induced in a broadband OPCPA; (2) whether OPP is space dependent or not when the pump intensity is nonuniform across the beam profile; and (3) whether there is a quantitative relationship between OPP and the linear phase shift, both of which are related with the crystal dispersion. Answers to these questions are essential to a deep understanding and experimental compensation of OPP, which have not been reported so far.

In this paper, we present a detailed theoretical investigation on OPP, including its nonlinear origin, feature, and compensation. We attribute OPP to the cascaded nonlinear phase in a broadband OPCPA, and also link the magnitude of OPP with the crystal dispersion. The paper is organized as follows. In Sec. II, we begin with the numerical model and the cascaded quadratic nonlinearity and then focus on discussing the nonlinear origin of OPP. In Secs. III and IV, we give detailed results for the feature and compensation of OPP, respectively. Finally, we summarize all the results in Sec. V.

II. NONLINEAR ORIGIN OF OPP

As a large linear chirp is imposed on the broadband signal pulse before it is launched onto the amplifier, OPCPA is a fairly special case in which all the three interacting waves are quasimonochromatic at each temporal slice. The local approximation stays satisfied under the condition of noncollinear PM (i.e., the group-velocity mismatch is negligible) [21,22]. A broadband OPCPA can be temporally sliced into a group of independent narrowband OPAs with their own instantaneous frequencies of signal and idler, while an integration of these narrowband OPAs gives the performance of broadband OPCPA. Naturally, the slowly varying envelope approximation, valid for narrowband OPAs, can be well applied to a broadband OPCPA. To numerically study OPP, here we adopt the standard coupled-wave equations derived

*majg@sjtu.edu.cn
†qianlj19@sjtu.edu.cn

under the slowly varying envelope approximation [23]. In fact, most numerical studies of broadband OPCPAs were based on such a standard approach [16–19,24–26], whose validity has been proven by experiments [17,18]. By taking the dispersion terms up to the fifth order, the coupled-wave equations that govern the OPCPA are given by

$$\begin{aligned}
&\frac{\partial A_s}{\partial z}+\frac{1}{2in_sk_s}\frac{\partial^2 A_s}{\partial x^2}-\sum_{j=2}^{j=5}\frac{(-i)^{j-1}}{j!}\beta_{js}\frac{\partial^j A_s}{\partial t^j}=i\frac{\omega_s d_{\text{eff}}}{n_s c}A_pA_i^*e^{-i\Delta k_0 z},\\
&\frac{\partial A_i}{\partial z}+\frac{1}{2in_ik_i}\frac{\partial^2 A_i}{\partial x^2}-\sum_{j=2}^{j=5}\frac{(-i)^{j-1}}{j!}\beta_{ji}\frac{\partial^j A_i}{\partial t^j}=i\frac{\omega_i d_{\text{eff}}}{n_i c}A_pA_s^*e^{-i\Delta k_0 z},\\
&\frac{\partial A_p}{\partial z}+\frac{1}{2in_pk_p}\frac{\partial^2 A_p}{\partial x^2}-\sum_{j=2}^{j=5}\frac{(-i)^{j-1}}{j!}\beta_{jp}\frac{\partial^j A_p}{\partial t^j}=i\frac{\omega_p d_{\text{eff}}}{n_p c}A_sA_ie^{i\Delta k_0 z}.
\end{aligned}\tag{1}$$

In these equations, all the linear effects of diffraction and dispersions are included in the left-hand side, and the quadratic nonlinear interactions are described in the right-hand side. In addition, both the temporal and spatial walk-off are neglected in the Eq. (1) because the broadband noncollinear PM configuration and relative thin crystal are assumed. The signal, idler, and pump are represented by s,i, and p, respectively, and their angular frequencies satisfy a relation of $\omega_p=\omega_s+\omega_i$ due to energy conservation. $\Delta k_0=k_s+k_i-k_p$ is the mismatch among their wave vectors at central frequencies. n is the crystal refractive index that follows the Sellmeier equation [27]. A is the electric field envelope scaled by $n^{1/2}$. d_{eff} is the effective nonlinear coefficient, determined by the quadratic nonlinear susceptibility $\chi^{(2)}(\omega_p;\omega_s,\omega_i)$ in OPA. In the simulations, up to the fifth-order dispersions are considered. The jth-order $(j=2-5)$ dispersion coefficient $\beta_j=\partial^{(j)}k/\partial\omega^{(j)}$ represents the group-velocity dispersion (GVD), third-order dispersion (TOD), fourth-order dispersion (FOD), and fifth-order dispersion, respectively.

To quantitatively study the performances of OPA and OPCPA, Eq. (1) was solved using the symmetric split-step Fourier algorithm [28]. Since the essential physics of OPP can be well revealed by a one-dimensional (1D) model in the time domain, we performed most of the following simulations with a simplified 1D model, except that the spatial effects have to be considered. In the simulations, the pump laser was assumed to be $I_p(x,t)=I_{p0}\exp[-(4\ln 2)(x/\sigma_p)^{2m}]\exp[-(4\ln 2)(t/\tau_p)^{2m}]$, where I_{p0} is the peak intensity and $\sigma_p=5\,\text{mm}(\tau_p=30\,\text{ps})$ is the beam width (pulse duration). Specifically, a temporally super-Gaussian ($m=4$) pump pulse was adopted in the 1D model, whereas a spatiotemporally Gaussian ($m=1$) pump laser was adopted in the two-dimensional model. In the broadband OPCPA, a Gaussian seed pulse with a FWHM bandwidth of $\Delta\nu=70\,\text{THz}$ was chirped to a duration of $\tau_s=10\,\text{ps}$. In the conventional monochromatic OPA, a Gaussian pump pulse with a duration of $\tau_p=10\,\text{ps}$ was used. In both cases, we assumed $d_{\text{eff}}=2\,\text{pm/V}$ and the crystal length of $L=5\,\text{mm}$. The pump intensities were set to $I_{p0}=4$ and $15\,\text{GW/cm}^2$, corresponding to small-signal parametric gains of $G_0=10^3$ and 10^7, respectively. For the calculations in Secs. II and III, the GVD and TOD values are assumed as $|\beta_2|=150\,\text{fs}^2/\text{mm}$ and $|\beta_3|=2000\,\text{fs}^3/\text{mm}$, both of which are typical for β-BBO or $LiNbO_3$ crystals in the commonly utilized wavelength regions.

The three-wave nonlinear interactions based on quadratic nonlinearity $\chi^{(2)}$ are usually associated with frequency conversion applications, such as second-harmonic generation (SHG) and OPA. Notably, the effective $\chi^{(3)}$ $(3\omega;\,\omega,\,\omega,\,\omega)$ due to cascading of $\chi^{(2)}$ $(3\omega;\,2\omega,\,\omega)$:$\chi^{(2)}$ $(2\omega;\,\omega,\,\omega)$ has widely been used in generating the third harmonic of laser beams using two crystals. On the other hand, it was identified that quadratic nonlinear processes can also induce nonlinear phase shifts [29–32]. For example, an equivalent nonlinear refraction $\chi^{(3)}$ $(\omega;\,\omega,\,\omega,\,\omega)$ can be obtained through $\chi^{(2)}$ $(\omega;\,2\omega,\,-\omega)$: $\chi^{(2)}$ $(2\omega;\,\omega,\,\omega)$ cascading, a combination of SHG based on $\chi^{(2)}$ $(2\omega;\,\omega,\,\omega)$, and its back-conversion of $\chi^{(2)}$ $(\omega;\,2\omega,\,-\omega)$. Such a cascaded nonlinearity can simply be achieved in a single crystal where both the processes of SHG and its back-conversion take place under the phase-mismatched situation. Because it involves sequential or cascaded quadratic processes, this is referred to the cascaded nonlinearity. In an OPA with phase-mismatch on the center frequencies ($\Delta k_0\neq 0$), the cascaded nonlinearity at signal frequency $\chi^{(3)}_{\text{eff}}(\omega_s)$ can be obtained through $\chi^{(2)}(\omega_s;\omega_p,-\omega_i)$: $\chi^{(2)}(\omega_p;\omega_s,\omega_i)$ cascading, a combination of OPA based on $\chi^{(2)}(\omega_s;\omega_p,-\omega_i)$, and its back-conversion of $\chi^{(2)}(\omega_p;\omega_s,\omega_i)$. The cascaded nonlinear phase at signal $\Delta\varphi^{NL}(\omega_s)$ can be analytically expressed by [31]

$$\Delta\varphi^{NL}(\omega_s)\approx\begin{cases}-\frac{\Delta k_0 L}{2}+\tan^{-1}\left\{\frac{\Delta k_0}{2g}\right\}, & (\Delta k_0<2g)\\ -\frac{g^2L}{\Delta k_0}, & (\Delta k_0>2g)\end{cases},\tag{2}$$

where $g=d_{\text{eff}}A_p(0)\sqrt{\omega_s\omega_i}/(c\sqrt{n_sn_i})$ is the gain coefficient, and $A_p(0)$ is the incident pump field. As clearly shown in Eq. (2), the cascaded nonlinearity is resulted from phase-mismatch and depends on the OPA gain.

To prove above analysis, we calculated and compared the induced phases at signal in both a narrowband and a broadband OPA according to Eq. (1). Note that the induced phase in a phase-mismatched narrowband OPA is the so-called cascaded nonlinear phase. The induced phases on signal are calculated by subtracting the linear dispersion phase from the total output signal phase. In other words, the induced phases are the phase imposed on the signal in the presence of a pump, which is vanished in the absence of a pump. In a narrowband OPA with negligible dispersion effects, the cascaded nonlinear phase only exists under the condition of phase-mismatch ($\Delta k_0\neq 0$). In the case of $\Delta k_0<2g$, the cascaded nonlinear

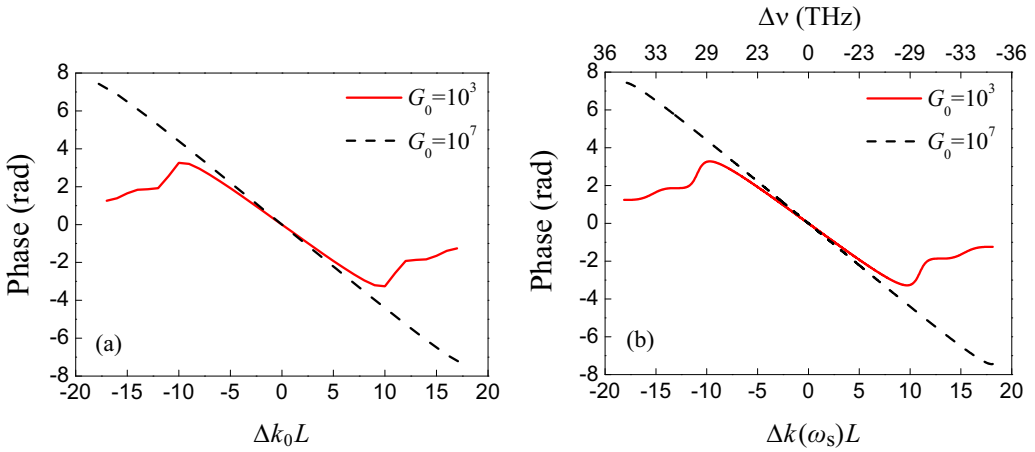

FIG. 1. Numerical results of the nonlinear phases produced in a narrowband OPA (a) and a broadband OPA (b). In both cases, the calculations are performed under two gain levels of 10^3 (red solid curves) and 10^7 (black dashed curves), respectively. The intrinsic phase-mismatch $\Delta k(\omega_s)$ in the broadband OPA is only contributed by idler dispersion ($\beta_{3i} = 2000\,\mathrm{fs}^3/\mathrm{mm}$). Throughout the calculations, the crystal length L is fixed at 5 mm and the incident signal intensity is set to be 10^{-10} of the pump intensity I_{p0}. The gain values of $G_0 = 10^3$ and $G_0 = 10^7$ are obtained by adjusting the pump intensities I_{p0} from 4 to $15\,\mathrm{GW/cm}^2$.

phase increases with Δk_0 and also increases with the OPA gain, as suggested by Eq. (2) and shown in Fig. 1(a). In a broadband ($\Delta\nu = 70\,\mathrm{THz}$) OPA with $\Delta k_0 = 0$, however, the similar nonlinear phase still presents, increases with the frequency deviation from the center frequency $\Delta k(\omega_s)$, and also increases with the gain [Fig. 1(b)]. When $\Delta k_0 > 2g$, the nonlinear phases in both a narrowband OPA and broadband OPA decrease with the increase of the phase-mismatches, as shown by the red solid curves in Fig. 1 and also implied by Eq. (2). In contrast to the phase-mismatch for the center frequencies Δk_0, we refer the phase-mismatch $\Delta k(\omega_s)$ due to crystal dispersions to the "intrinsic phase-mismatch." Such an intrinsic phase-mismatch $\Delta k(\omega_s)$ can be simply expressed by

$$\Delta k(\omega_s) = \Delta k_0 + \frac{\partial \Delta k}{\partial \omega_{s0}}\Delta\omega + \frac{1}{2}\frac{\partial^2 \Delta k}{\partial \omega_{s0}^2}(\Delta\omega)^2 + \frac{1}{6}\frac{\partial^3 \Delta k}{\partial \omega_{s0}^3}(\Delta\omega)^3 \cdots$$
$$= \frac{1}{2}(\beta_{2s} + \beta_{2i})(\Delta\omega)^2 + \frac{1}{6}(\beta_{3s} - \beta_{3i})(\Delta\omega)^3 \cdots . \quad (3)$$

We neglect both the zero-order and the first-order terms in above equation because a typical broadband OPA in the non-collinear PM configuration satisfies both the phase matching ($\Delta k_0 = 0$) and the group-velocity matching ($\partial \Delta k/\partial \omega_{s0} = 0$) conditions [33,34]. $\Delta\omega$ denotes the frequency detuning of the signal and can be expressed as $\Delta\omega = at$ for linearly chirped pulses with a chirp coefficient a. As shown in the Eq. (3), the intrinsic phase-mismatch $\Delta k(\omega_s)$ is contributed by the linear crystal dispersions at both signal and idler wavelengths. Even if there is no linear crystal dispersion at the signal wavelength (i.e., $\beta_{js} = 0, j = 2,3\ldots$), the signal may still experience a nonlinear phase due to the intrinsic phase-mismatch induced by the linear idler dispersion [Fig. 1(b)]. As a narrowband pump pulse was assumed ($\Delta\omega_p < \Delta\omega$), the idler frequency ($\omega_{i0} - \Delta\omega$) has a one-to-one correspondence to the signal frequency ($\omega_{s0} + \Delta\omega$), which ensures an equal spectrum for the idler and signal. Because the intrinsic phase-mismatch $\Delta k(\omega_s)$ is frequency dependent, the nonlinear phase manifests itself as a nonlinear spectral phase [Fig. 1(b)]. Notably, the nonlinear spectral phase in a broadband OPA exhibits a same value to the cascaded nonlinear phase in a narrowband OPA with $\Delta k_0 = \Delta k(\omega_s)$, which suggests that the nonlinear spectral phase induced by the intrinsic phase-mismatch $\Delta k(\omega_s)$ can be attributed to the cascaded nonlinear phase.

From the above discussions, it is clear that both the phase-mismatch for center frequencies ($\Delta k_0 \neq 0$) and intrinsic phase-mismatch [$\Delta k(\omega_s) \neq 0$] can induce the cascaded nonlinear phase shift in OPA. Next, we discuss the OPP in a broadband OPCPA and link OPP with the cascaded nonlinearity. The OPP in OPCPA was identified as the cascaded nonlinear phase in the following procedure: first, the OPP in a broadband phase-matched OPCPA ($\Delta k_0 = 0$), as defined by previous works [16], was directly calculated by using Eq. (1) with a seed signal in the form of chirped pulses; second, as suggested by the local approximation [21,22], a broadband OPCPA was viewed as an integration of a series of narrowband OPAs in the domain of time (t) or frequency (ω_s), each of which corresponds to an incident signal with an instantaneous frequency $\omega_s(t)$, a slice of pump pulse $A_p(t)$, and a phase-mismatch given by Eq. (3). The cascaded nonlinear phases of these OPAs were then calculated and compared with the OPP. In the numerical calculations, the OPP and cascaded nonlinear phase were obtained by subtracting the initially imposed phase (chirp) from the one after amplification.

To simplify the discussion on OPP, we first consider the crystal case with only idler TOD ($\beta_{3i} = 2000\,\mathrm{fs}^3/\mathrm{mm}$) where the signal will not experience a linear propagation phase from the crystal dispersion. Both the OPP and cascaded nonlinear phase were studied for two different parametric gains, as shown in Figs. 2(a) and 2(b). By viewing OPCPA as a series of narrowband OPAs as mentioned above, it is clear that there is a spectral distribution of cascaded nonlinear phases contributed by the intrinsic phase-mismatch [$\Delta k(\omega_s) \neq 0$]. On the other hand, the OPP in OPCPA, directly calculated by solving Eq. (1), also presents as a spectral phase with a zero value at the signal center frequency, where the phase

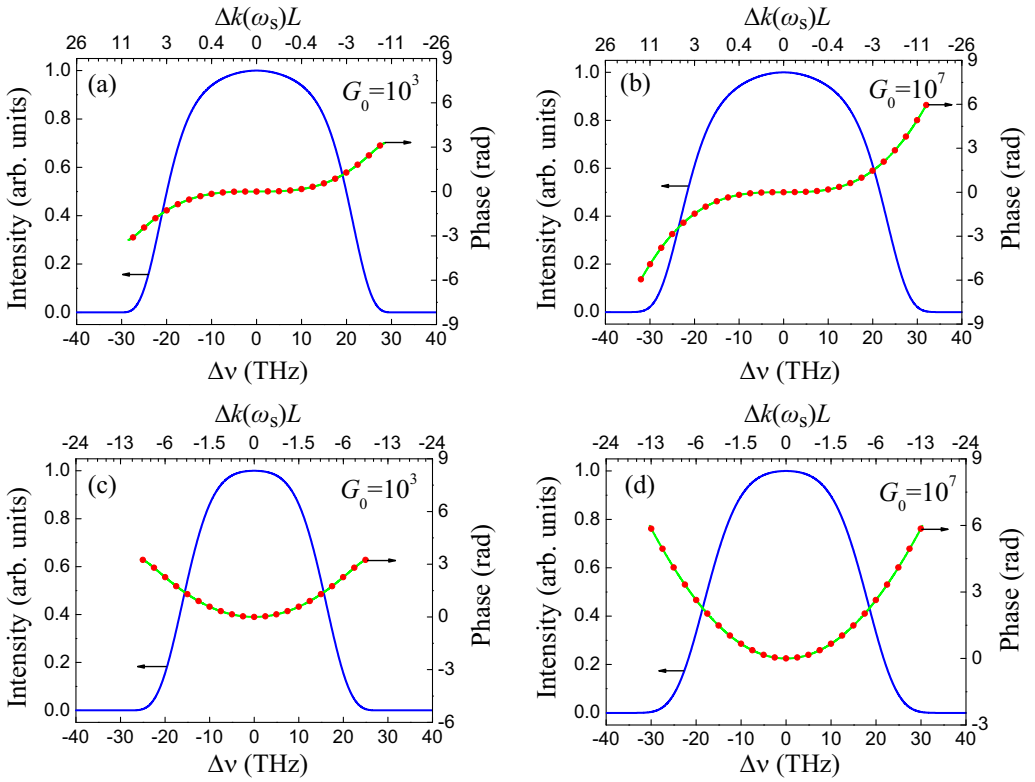

FIG. 2. Comparison of OPP (green solid curves) and cascaded nonlinear phase (red scatters). (a) The calculated OPP and cascaded nonlinear phase in an OPCPA with a third-order dispersion of idler ($\beta_{3i} = 2000\,\mathrm{fs}^3/\mathrm{mm}$) and low gain ($G_0 = 10^3$). (b) Same as (a), but in the case of high gain ($G_0 = 10^7$). (c) The calculated OPP and cascaded nonlinear phase in an OPCPA with a second-order dispersion of idler ($\beta_{2i} = -150\,\mathrm{fs}^2/\mathrm{mm}$) and low gain ($G_0 = 10^3$). (d) Same as (c), but in the case of high gain ($G_0 = 10^7$). The intrinsic phase-mismatch of OPCPA is also labeled in all figures, which is directly related to the cascaded nonlinear phase. In all the calculations, the bandwidth of incident signal is fixed at 70 THz, and other parameters are the same as their counterparts in Fig. 1.

matching is exactly satisfied [$\Delta k(\omega_{s0}) = 0$], and increases with the intrinsic phase-mismatch [$\Delta k(\omega_s) \neq 0$] as well as the parametric gain G_0. It is interesting that the OPP in OPCPA matches exactly to the cascaded nonlinear spectral phase in the quantity, and both their signs are opposite to the intrinsic phase-mismatch as suggested by Eq. (2). The above discussions lead us to conclude that the OPP induced in a broadband OPCPA can be attributed to the cascaded nonlinear phase. We further studied the crystal case with a GVD at idler ($\beta_{2i} = -150\,\mathrm{fs}^2/\mathrm{mm}$) and confirmed the conclusion again [Figs. 2(c) and 2(d)].

In the crystal case with only idler dispersion, such as those considered above, the amplified signal does not experience a linear crystal dispersion. For a better understanding of the signal phase after amplification, here we consider a crystal situation with only signal dispersion, where the amplified signal will experience both the crystal dispersion and OPP. The simulation results are summarized in Fig. 3. We first calculated the total output signal phase after amplification, which has an identical sign and a smaller quantity compared to the linear propagation phase. The difference between them is OPP resulting from the cascade nonlinearity in a broadband OPCPA. In the crystal case with a normal GVD [Fig. 3(a)] and TOD at the signal [Fig. 3(b)], the generated negative OPP will partly counteract the positive linear phase, resulting in a relatively smaller output signal phase. In the crystal case with an anomalous signal dispersion, both the OPP and linear propagation phase will just change their signs accordingly, thus also resulting in a smaller output signal phase. On the other hand, the obtained OPP here is exactly the same as its counterpart in Fig. 2 if the idler dispersion is set for a same intrinsic phase-mismatch as that contributed by the signal dispersion. Therefore, we can generally conclude that the output signal phase after amplification is a sum of the linear propagation phase in the crystal and the cascaded nonlinear phase (i.e., OPP) induced in amplification.

III. FEATURES OF OPP

In this section, we study the influences of the small-signal gain and pump depletion on OPP. To quantitatively illustrate the OPP and link it to the various orders of linear crystal dispersion, we expand the calculated OPP around the central signal frequency similar to Eq. (3),

$$\varphi(\omega_s) = \varphi(\omega_{s0}) + \alpha_1(\Delta\omega) + \tfrac{1}{2}\alpha_2(\Delta\omega)^2 + \tfrac{1}{6}\alpha_3(\Delta\omega)^3 + \cdots, \tag{4}$$

where $\alpha_j = \partial^{(j)}\varphi/\partial\omega^{(j)}$ is the jth-order OPP. In the following calculations, we employ a parameter $\alpha_j/(\beta_j L)$ to characterize the amount of OPP. For example, $\alpha_3/(\beta_{3i} L)$ indicates the ratio of third-order OPP to the crystal TOD at idler.

First, we study the influence of the small-signal gain G_0 on OPP (Fig. 4). The dependence of OPP on gain G_0 in the case

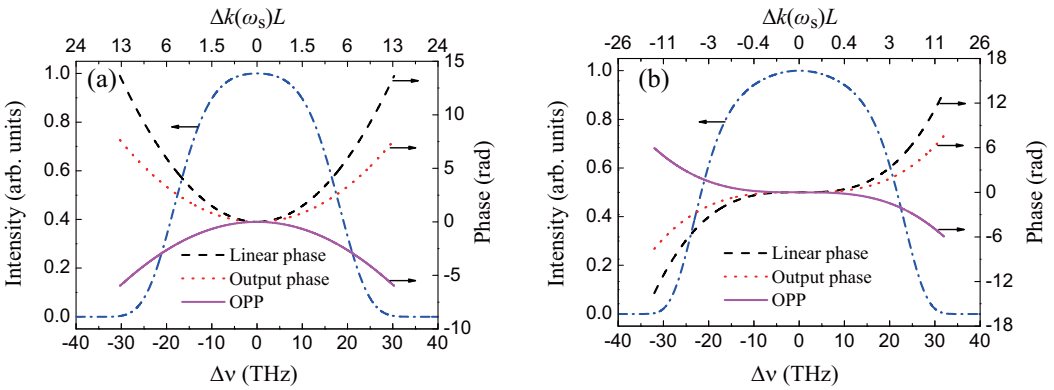

FIG. 3. Comparison among the linear phase (black dashed curves), the output phase after amplification (red dotted curves), and OPP (purple solid curves) for different signal dispersions. In (a), $\beta_{2s} = 150\,\mathrm{fs}^2/\mathrm{mm}$, and in (b), $\beta_{3s} = 2000\,\mathrm{fs}^3/\mathrm{mm}$. The signal bandwidth and OPCPA gain are 70 THz and $G_0 = 10^7$, respectively, and the other parameters are the same as their counterparts in Fig. 2.

of signal GVD [blue solid curve in Fig. 4(a)] is the same as that of signal TOD [blue solid curve in Fig. 4(b)]. Moreover, the phase characteristic of OPP is the same as that of the imposed crystal dispersion but exhibits an opposite sign. Taking the signal GVD case as an example, the generated OPP presents a phase characteristic as like the GVD-resulted linear phase, i.e., the OPP can be fully characterized by the second-order phase term (α_2) in Eq. (4) that has a characteristic the same as GVD. The OPP magnitude increases with G_0 and approaches to half the signal dispersion in the high-gain regime (e.g., $G_0 > 10^5$). In the crystal case with idler GVD [red dashed curve in Fig. 4(a)], a similar conclusion is expected, i.e., the OPP has a same phase characteristic and opposite sign with those of the linear idler dispersion. However, in the crystal case with idler TOD [red dashed curve in Fig. 4(b)], the OPP has a same sign with the linear idler dispersion even though they show a same phase characteristic. Such a rule of OPP signs can be easily understood by Eq. (3), where the idler TOD has an opposite contribution compared to that of the signal TOD. In summary, a general conclusion can be deduced that the OPP magnitude in the high-gain limit is nearly half the intrinsic phase-mismatch, i.e., $\varphi(\omega_s) \approx -\Delta k(\omega_s)L/2$.

Second, we study the influence of pump depletion on OPP by adjusting the seed signal intensity [Fig. 5(a)]. Because a high gain of $G_0 = 10^7$ was adopted in the simulations, the OPP is nearly half the imposed idler GVD and remains unchanged with varied seed signals until significant back-conversion occurs. In the strong seeding regime ($I_s/I_{p0} \geqslant 10^{-4}$) where the OPCPA efficiency is severely degraded by the effect of back-conversion, the OPP magnitude can dramatically deviate from that in a conventional OPCPA. This is because that the OPP characteristic (i.e., the phase profile in the spectral domain) will be distorted by the back-conversion effect and thus no longer determined by a single parameter α_2. As shown in Fig. 5(b), the profile of OPP in the strong seeding regime is severely deviated from a α_2-determined parabolic shape. Actually, in this situation, there are higher-order dispersion components in the distorted OPP, and an extension up to the sixth-order term will give a better fitting to the OPP.

Finally, we study the spatial dependence of OPP. As discussed in Sec. II, the OPP magnitude is determined by the parametric gain and thus might be spatially dependent when the pump beam is nonuniform. A spatiotemporal two-dimensional code and a Gaussian pump beam with $\sigma_p = 5$ mm were used in the calculations. Figure 6 depicts the distributions of spectrum and phase in the crystal case with only idler dispersion. While OPP in the spectral domain [Figs. 6(b) and 6(c)] is quite similar to those calculated by using a 1D code, the OPP in the spatial domain [Figs. 6(b) and 6(d)] is surprisingly independent of space. For instance, the two OPP

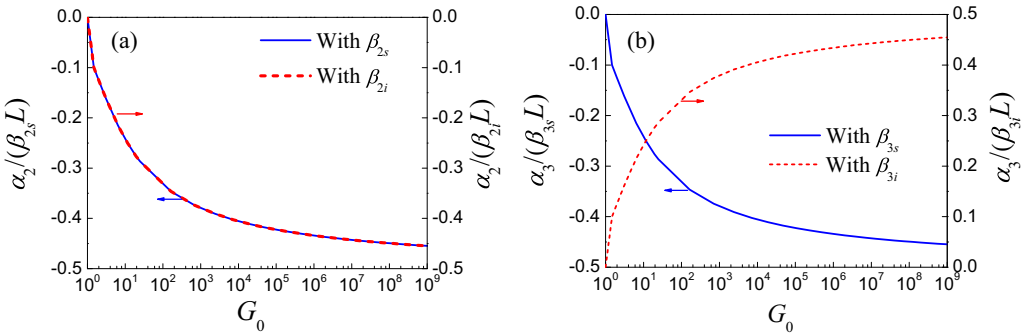

FIG. 4. The OPP coefficient (normalized to the imposed crystal dispersion) versus small-signal gain G_0. In (a), $\beta_{2s} = 150\,\mathrm{fs}^2/\mathrm{mm}$ (blue solid curve) and $\beta_{2i} = -150\,\mathrm{fs}^2/\mathrm{mm}$ (red dashed curve). In (b), $\beta_{3s} = 2000\,\mathrm{fs}^3/\mathrm{mm}$ (blue solid curve) and $\beta_{3i} = 2000\,\mathrm{fs}^3/\mathrm{mm}$ (red dashed curve). In the simulations, the pump intensity was varied from 0.1 to 25 $\mathrm{GW/cm}^2$ to adjust the small-signal gain G_0 from 1 to 10^9, and the signal intensity was fixed at 0.1 $\mathrm{W/cm}^2$ to maintain the pump undepleted. The other parameters are the same as their counterparts in Fig. 2.

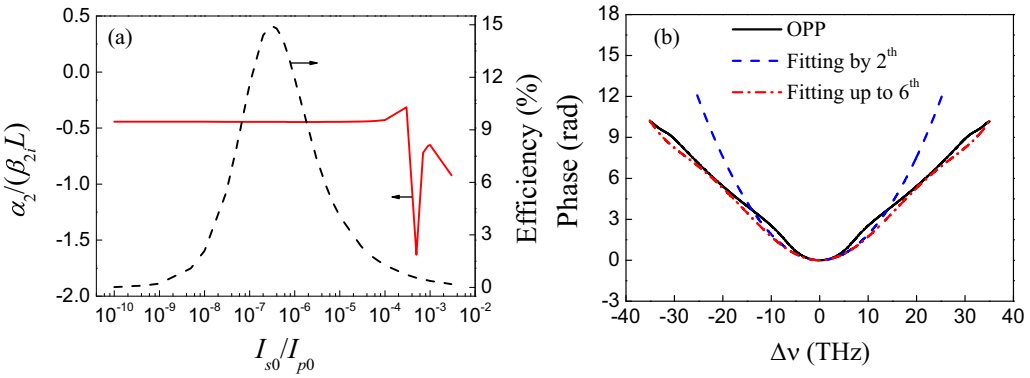

FIG. 5. (a) OPP (red solid curve) and OPCPA efficiency (black dashed curve) versus seeding signal intensity under the conditions of $G_0 = 10^7$ and $\beta_{2i} = -150\,\mathrm{fs}^2/\mathrm{mm}$. (b) The generated OPP at $I_{s0}/I_{p0} = 5 \times 10^{-4}$ (black solid curve) and its fitting by only second-order terms (blue dashed curve) and up to sixth-order terms (red dash-dotted curve).

values at the beam center ($x/\sigma_s = 0$) and beam edge ($x/\sigma_s = 0.2$) are almost identical, despite that the pump intensities at these two positions are largely different [Fig. 6(c)]. Such an interesting feature of OPP can be simply understood by the result shown in Fig. 4(a): in the high-gain limit, the OPP approaches to a constant value of half the imposed crystal dispersion. For the same reason, the OPP values at a fixed frequency ($\Delta\nu/\Delta\nu_0 = 0$ or $\Delta\nu/\Delta\nu_0 = 0.25$) are also nearly constant in the spatial domain [Fig. 6(d)].

IV. COMPENSATION OF OPP

In previous sections, the nonlinear origin of OPP and its magnitude have been studied, which will significantly degrade pulse compression in the few-cycle pulse regime. Here, we study the OPP and its compensation in a typical noncollinear OPCPA system based on a β-BBO crystal. The major simulation parameters are listed in Table I. In this case, the residual phase-mismatches up to a fifth-order term ($\partial\Delta k/\partial\omega_{s0}, \partial^2\Delta k/\partial\omega_{s0}^2, \partial^3\Delta k/\partial\omega_{s0}^3, \partial^4\Delta k/\partial\omega_{s0}^4$

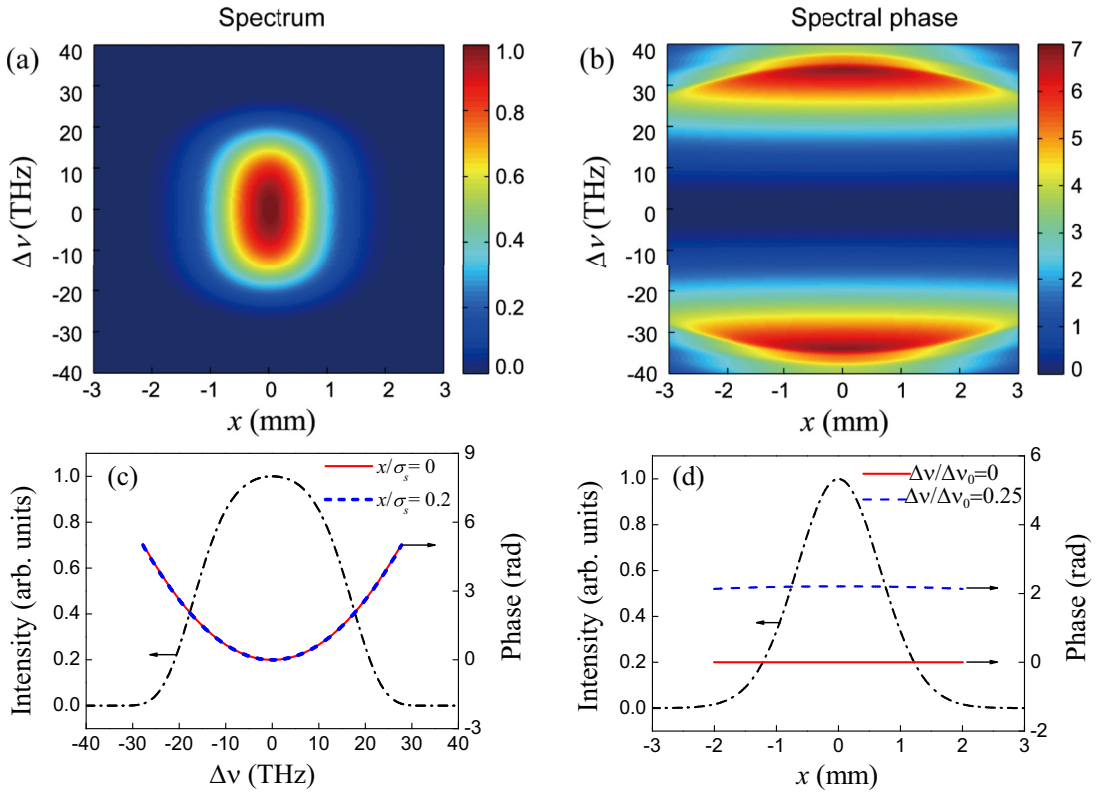

FIG. 6. Spatio-spectral distributions of signal and its phase under the conditions of $G_0 = 10^7$ and $\beta_{2i} = -150\,\mathrm{fs}^2/\mathrm{mm}$. (a) Amplified signal in the spatio-spectral domain. (b) OPP in the spatio-spectral domain. (c) OPP in the spectral domain. (d) OPP in the spatial domain. Other parameters are the same as their counterparts in Fig. 2.

TABLE I. The simulation parameters for a noncollinear OPCPA in a β-BBO crystal.

	Parameter	Value
Seed	Central wavelength	800 nm
	Frequency bandwidth ($\Delta\nu$)	70 THz
	Temporal chirp coefficiect (a)	44 ps^{-2}
	Input intensity	4.5 kW/cm^2
Pump	Wavelength	532 nm
	Intensity	15 GW/cm^2
β-BBO	Length	5 mm
	Phase-matching angle (θ)	23.96°
	Noncollinear angle between signal and pump	2.48°

and $\partial^5\Delta k/\partial\omega_{s0}^5$) were calculated to be 0 fs/mm, $-20\,fs^2/mm$, $-358\,fs^3/mm$, $-1583\,fs^4/mm$, and $-9642\,fs^5/mm$, respectively. The transverse effects were neglected in the simulations by assuming a relatively large beam width (i.e., 5 mm).

Figure 7(a) shows the amplified signal spectrum and its spectral phase induced by the OPCPA process. Here, we assume that the pulse compressor cancels the dispersion imposed by the stretcher and also the GVD of the β-BBO crystal. The OPP is quite flat around the central frequency and is dominated by TOD and higher-order dispersions because both the group-velocity mismatch and GVD can be neglected in the noncollinear PM configuration. On the other hand, as discussed in the previous sections, the generated OPP in the high-gain ($G_0 = 10^7$) situation is nearly half the intrinsic phase-mismatch due to crystal dispersion. In addition, because of a large PM bandwidth (~100 THz) in the noncollinear configuration, the amplified signal spectrum is broadened from its incident value of 70 THz to 92 THz, which may support a Fourier-transform (FT) limited pulse duration of ~8 fs, as shown in Fig. 7(b). The presence of OPP results in a longer compressed pulse of ~11 fs and a ~36% reduction of peak intensity. Thus, it is necessary to compensate OPP in a practical few-cycle OPCPA system.

We study the compensation of OPP up to the third-order, fourth-order, and fifth-order dispersion, respectively. As expected, OPP compensation can significantly improve the pulse compression and thus the peak intensity. Figures 7(c) and 7(d) present the residual spectral phases and the corresponding compressed pulses after compensating OPP, respectively. In the case with OPP compensation up to the third-order (the fourth-order) term, a pulse duration of ~9.5 fs (~8.5 fs) can be achieved with a peak intensity improved by ~21% (~25%). The OPP can be fully compensated by dispersion compensation up to the fifth-order term, which corresponds to a FT-limited pulse of ~8 fs after pulse compression. The results show that the OPP compensation needs additional management of TOD and even higher-order dispersions in few-cycle OPCPA systems, even though the noncollinear PM configuration is employed.

V. CONCLUSIONS

In a broadband OPCPA system, the nonlinear spectral phase, termed as OPP, is inevitably produced by the intrinsic

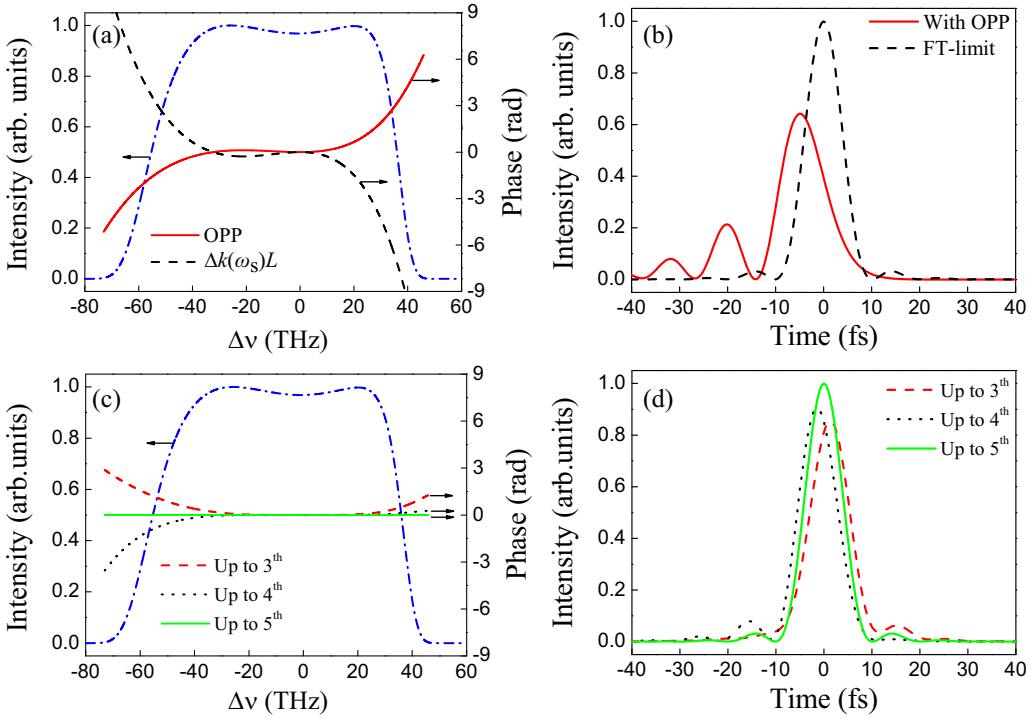

FIG. 7. The OPP and its compensation in a practical noncollinear OPCPA system based on a β-BBO crystal. (a) Amplified signal spectrum (blue dash-dotted curve), the generated OPP (red solid curve) and the intrinsic phase-mismatch $\Delta k(\omega_s)L$ in the β-BBO crystal (black dashed curve). (b) Compressed pulse (red solid curve) and the Fourier-limited pulse (black dashed curve). (c) Residual phases after dispersion compensation up to TOD (red dashed curve), FOD (black dotted curve), and the fifth-order dispersion (green solid curve), respectively. (d) The corresponding compressed pulses to the cases in (c).

phase-mismatch due to crystal dispersions. By viewing OPCPA as a series of narrowband OPAs in the time domain with individual signal instantaneous frequencies, we have linked OPP to the cascaded nonlinear phase shifts due to intrinsic phase-mismatch and verified that OPP originates from the cascaded quadratic nonlinearity. Based on the numerical studies, we have shown that the phase characteristic of OPP is the same as that of the imposed crystal dispersion. The total output signal phase after amplification is a sum of OPP and the linear propagation phase in the crystal. In the crystal case with signal dispersion, the OPP and linear crystal dispersion always have opposite signs, and thus they can be partially compensated to each other. In the limit of high parametric gain, the OPP magnitude can be simply linked to the crystal dispersion, which is nearly half the intrinsic phase-mismatch. According to the study on a typical noncollinear OPCPA system based on a β-BBO crystal, the OPP can significantly affect the pulse compression and thus necessitates an additional dispersion compensation of signal pulses. According to the quantitative relationship between OPP and the crystal dispersion in the high-gain regime, the effect of OPP in the spatial domain is negligible, which makes the OPP compensation necessary only in the spectral domain. The results presented in this paper will be crucial to a deep understanding and experimental compensation of OPP, which may further promote the progress of few-cycle intense pulses.

ACKNOWLEDGMENTS

This work was supported by the National Basic Research Program of China (Grant No. 2013CBA01505), National Natural Science Foundation of China (Grant No. 11421064), and Science and Technology Commission of Shanghai Municipality (Grants No. 15XD1502100, No. 17YF1409100, and No. 17ZR1414000).

[1] F. Krausz and M. Ivanov, Attosecond physics, Rev. Mod. Phys. **81**, 163 (2009).

[2] E. Goulielmakis, M. Schultze, M. Hofstetter, V. S. Yakovlev, J. Gagnon, M. Uiberacker, A. L. Aquila, E. M. Gullikson, D. T. Attwood, R. Kienberger, F. Krausz, and U. Kleineberg, Single-cycle nonlinear optics, Science **320**, 1614 (2008).

[3] A. Baltuška, Th. Udem, M. Uiberacker, M. Hentschel, E. Goulielmakis, Ch. Gohle, R. Holzwarth, V. S. Yakovlev, A. Scrinzi, T. W. Hänsch, and F. Krausz, Attosecond control of electronic processes by intense light fields, Nature (London) **421**, 611 (2003).

[4] A. Dubietis, G. Jonušauskas, and A. Piskarskas, Powerful femtosecond pulse generation by chirped and stretched pulse parametric amplification in BBO crystal, Opt. Commun. **88**, 437 (1992).

[5] H. Fattahi, H. G. Barros, M. Gorjan, T. Nubbemeyer, B. Alsaif, C. Y. Teisset, M. Schultze, S. Prinz, M. Haefner, M. Ueffing *et al.*, Third-generation femtosecond technology, Optica **1**, 45 (2014).

[6] G. M. Gale, M. Cavallari, T. J. Driscoll, and F. Hache, Sub-20-fs pulses in the visible from an 82-MHz optical parametric oscillator, Opt. Lett. **20**, 1562 (1995).

[7] G. Cerullo, M. Nisoli, and S. D. Silvestri, Generation of 11 fs pulses tunable across the visible by optical parametric amplification, Appl. Phys. Lett. **71**, 3616 (1997).

[8] A. Shirakawa and T. Kobayashi, Noncollinearly phase-matched femtosecond optical parametric amplification with a 2000 cm^{-1} bandwidth, Appl. Phys. Lett. **72**, 147 (1998).

[9] D. Herrmann, L. Veisz, R. Tautz, F. Tavella, K. Schmid, V. Pervak, and F. Krausz, Generation of sub-three-cycle, 16 TW light pulses by using noncollinear optical parametric chirped-pulse amplification, Opt. Lett. **34**, 2459 (2009).

[10] N. Ishii, K. Kaneshima, K. Kitano, T. Kanai, S. Watanabe, and J. Itatani, Sub-two-cycle, carrier-envelop phase-stable, intense optical pulses at 1.6 μm from a BiB_3O_6 optical parametric chirped-pulse amplifier, Opt. Lett. **37**, 4182 (2012).

[11] Y. Deng, A. Schwarz, H. Fattahi, M. Ueffing, X. Gu, M. Ossiander, T. Metzger, V. Pervak, H. Ishizuki, T. Taira *et al.*, Carrier-envelop-phase-stable, 1.2 mJ, 1.5 cycle laser pulses at 2.1 μm, Opt. Lett. **37**, 4973 (2012).

[12] B. E. Schmidt, N. Thiré, M. Boivin, A. Laramée, F. Poitras, G. Lebrun, T. Ozaki, H. Ibrahim, and F. Légaré, Frequency domain optical parametric amplification, Nat. Commun. **5**, 3643 (2014).

[13] G. Porat and A. Arie, Efficient, broadband and robust frequency conversion by fully nonlinear adiabatic three wave mixing, J. Opt. Soc. Am. B **30**, 1342 (2013).

[14] O. Yaakobi, L. Caspani, M. Clerici, F. Vidal, and R. Morandotti, Complete energy conversion by autoresonant three-wave mixing in nonuniform media, Opt. Express, **21**, 1623 (2013).

[15] J. Ma, J. Wang, P. Yuan, G. Xie, K. Xiong, Y. Tu, X. Tu, E. Shi, Y. Zheng, and L. Qian, Quasi-parametric amplification of chirped pulses based on a Sm^{3+}-doped yttrium calcium oxyborate crystal, Optica **2**, 1006 (2015).

[16] I. N. Ross, P. Matousek, G. H. C. New, and K. Osvay, Analysis and optimization of optical parametric chirped pulse amplification, J. Opt. Soc. Am. B **19**, 2945 (2002).

[17] S. Demmler, J. Rothhardt, S. Hädrich, J. Bromage, J. Limpert, and A. Tünnermann, Control of nonlinear spectral phase induced by ultrabroadband optical parametric amplification, Opt. Lett. **37**, 3933 (2012).

[18] A. Renault, D. Z. Kandula, S. Witte, A. L. Wolf, R. Th. Zinkstok, W. Hogervorst, and K. S. E. Eikema, Phase stability of terawatt-class ultrabroadband parametric amplification, Opt. Lett. **32**, 2363 (2007).

[19] D. Herrmann, C. Homann, R. Tautz, M. Scharrer, P. St. J. Russell, F. Krausz, L. Veisz, and E. Riedle, Approaching the full octave noncollinear optical parametric chirped pulse amplification with two-color pumping, Opt. Express **18**, 18752 (2010).

[20] J. Ma, J. Wang, D. Hu, P. Yuan, G. Xie, H. Zhu, H. Yu, H. Zhang, J. Wang, and L. Qian, Theoretical investigations of broadband mid-infrared optical parametric amplification based on a $La_3Ga_{5.5}Nb_{0.5}O_{14}$ crystal, Opt. Express **24**, 23957 (2016).

[21] J. Moses and S-W. Huang, Conformal profile theory for performance scaling of ultrabroadband optical parametric chirped pulse amplification, J. Opt. Soc. Am. B **28**, 812 (2011).

[22] E. J. Grace, C. L. Tsangaris, and G. H. C. New, Competing processes in optical parametric chirped pulse amplification, Opt. Commun. **261**, 225 (2006).

[23] S. Witte and K. S. E. Eikema, Ultrafast optical parametric chirped-pulse amplification, IEEE J. Quantum Electron. **18**, 296 (2012).

[24] M. J. Prandolini, R. Riedel, M. Schulz, A. Hage, H. Hoppner, and F. Tavella, Design considerations for a high power, ultrabroadband optical parametric chirped-pulse amplifier, Opt. Express **22**, 1594 (2014).

[25] D. Herrmann, R. Tautz, F. Tavella, F. Kausz, and L. Veisz, Investigation of two-beam-pumped noncollinear optical parametric chirped-pulse amplification for the generation of few-cycle light pulse, Opt. Express **18**, 4170 (2010).

[26] A. Thai, C. Skrobol, P. K. Bates, G. Arisholm, Z. Major, F. Krausz, S. Karsch, and J. Biegert, Simulations of petawatt-class few-cycle optical parametric chirped-pulse amplification including nonlinear refractive index effects, Opt. Lett. **35**, 3471 (2010).

[27] D. N. Nikogosyan, *Nonlinear Optical Crystals: A Complete Survey* (Springer, New York, 2005).

[28] F. Tavella, A. Marcinkevičius, and F. Krausz, Investigation of the superfluorescence and signal amplification in an ultrabroadband multiterawatt optical parametric chirped pulse amplifier system, New J. Phys. **8**, 219 (2006).

[29] R. Desalvo, H. Vanherzeele, D. J. Hagan, M. Sheik-Bahae, G. Stegeman, and E. W. VanStryland, Self-focusing and self-defocusing by cascaded second-order effects in KTP, Opt. Lett. **17**, 28 (1992).

[30] G. I. Stegeman, M. S-Bahae, E. Van Stryland, and G. Assanto, Large nonlinear phase shifts in second-order nonlinear optical processes, Opt. Lett. **18**, 13 (1993).

[31] H. J. Bakker, P. C. M. Planken, L. Kuipers, and A. Lagendijk, Phase modulation in second-order nonlinear-optical processes, Phys. Rev. A **42**, 4085 (1990).

[32] P. C. M. Planken, H. J. Bakker, L. Kuipers, and A. Lagendijk, Efficient, frequency chirp in optical parametric amplification with large phase mismatch in noncentrosymmetric crystals, J. Opt. Soc. Am. B **7**, 2150 (1990).

[33] E. Riedle, M. Beutter, S. Lochbrunner, J. Piel, S. Schenkl, S. Sporlein, and W. Zinth, Generation of 10 to 50 fs pulses tunable through all of the visible and the NIR, Appl. Phys. B **71**, 457 (2000).

[34] T. Wilhelm, J. Piel, and E. Riedle, Sub-20-fs pulses tunable across the visible from a blue-pumped single-pass noncollinear parametric converter, Opt. Lett. **22**, 1494 (1997).